Research paper

Synthesis and characterizations of metal-free Semiconductor/MOFs with good stability and high photocatalytic activity for H$_2$ evolution: A novel Z-Scheme heterostructured photocatalyst formed by covalent bonds

Gang Zhou[a], Mei-Feng Wu[a], Qiu-Ju Xing[a], Fei Li[a], Hui Liu[b,c], Xu-Biao Luo[a], Jian-Ping Zou[a,*], Jin-Ming Luo[d,*], Ai-Qin Zhang[a]

[a] Key Laboratory of Jiangxi Province for Persistent Pollutants Control and Resources Recycle, Nanchang Hangkong University, Nanchang 330063, PR China
[b] Department of Environmental Engineering, School of Metallurgy and Environment, Central South University, Changsha, Hunan, PR China
[c] Chinese National Engineering Research Centre for Control and Treatment of Heavy Metal Pollution, Changsha, Hunan, PR China
[d] Brook Byers Institute for Sustainable Systems and School of Civil and Environmental Engineering, Georgia Institute of Technology, Atlanta, GA, 30332, United States

ARTICLE INFO

ABSTRACT

To solve serious energy and environmental crises caused by rapid industrial development, the formation of Z-scheme heterostructured photocatalysts is a promising approach for efficient and scalable H$_2$ production from water splitting due to wide absorption range, high charge-separation efficiency and strong redox ability of the Z-scheme heterostructured photocatalysts. In this study, we combined the MOFs of NH$_2$-MIL-125(Ti) with g-C$_3$N$_4$ functionalized by benzoic acid (CFB) to synthesize a novel composite catalyst of CFB/NH$_2$-MIL-125(Ti) (CFBM) by covalent bonds for the first time. The benzoic acid in the CFBM acts as electron mediator to well separate photogenerated electrons and holes, leading to excellent photocatalytic performance of photocatalytic hydrogen generation from water splitting under visible light irradiation. Experimental results show that the H$_2$ production rate of the 10CFBM is 1.123 mmol·h^{-1}·g^{-1}, which is about 6 times of the NH$_2$-MIL-125(Ti). Meanwhile, the simple physical mixture of NH$_2$-MIL-125(Ti) with 10 wt% g-C$_3$N$_4$ and the 10wt%g-C$_3$N$_4$/MOFs heterostructured catalyst all show much smaller H2 evolution rate and worse stability than that of the 10CFBM. Finally, we proposed a possible mechanism to well explain the improved photocatalytic performance of the Z-scheme photocatalytic system based on the results of different characterizations. The present work gives a good example to develop a novel Z-scheme heterostructured system with good stability and high photocatalytic activity for H$_2$ evolution and puts forward a new synthetic strategy to prepare metal-free semiconductor/MOFs formed by covalent bonds.

1. Introduction

With the rapid consumption of nonrenewable fossil fuels, human beings are facing the challenge of energy crisis and environmental pollution [1–4]. Environmental friendly and sustainable energy (wind energy, water energy and solar energy) is constantly being developed and utilized, in which the solar energy has been favored by the majority of researchers and widely used in human life. Photocatalytic hydrogen generation from water would replace the traditional fossil fuels as its environmental friendly and facile use of solar energy [5–13]. Metal-organic frameworks (MOFs), consisting of organic linkers and metal-oxo clusters, have been widely investigated and applied in molecular sensing, drug delivery, gas storage/separation, and photocatalysis [14–18] due to the advantages of high specific surface area, adjustable pore size, high crystal structure and easy modification of surface [19–23]. However, there were still some drawbacks for pure MOFs, such as low photoresponsivity, high recombination rate of photogenerated electron-hole pairs and poor stabilities, leading to low efficiency of visible light utilization and low photocatalytic performance of MOFs [24,25]. To improve the photocatalytic activities of pure MOFs, many researchers coupled MOFs (NH$_2$-MIL-125(Ti), UiO-66 [25] and ZIF-9 [26]) with semiconductor compounds such as TiO$_2$ [27], CdS [28], Fe$_3$O$_4$ [29], MoS$_2$ [5], Ag [30], Au [31], Pt [32], Pd [33], and Co [16] to form hybrid materials with good light absorption and photocatalytic efficiency [34–36]. However, to the best of our knowledge, metal-free semiconductors are rarely used in the hybrid materials of semiconductor/MOFs. And most of the hybrid materials of semiconductor/MOFs are used to degrade organic pollutants [37] or remove

---

heavy metal ions from wastewater, but few of them were reported for the photocatalytic hydrogen evolution [25,38]. Furthermore, among the hybrid materials, the junctions between semiconductor and MOFs are generally via weak van der Waals force or hydrogen bonds, which results in bad stability and low separation rate of the photogenerated electrons and holes of the hybrid materials. Therefore, it is urgent to prepare some novel heterostructured catalysts of semiconductor/MOFs that were connected by strong bond force between semiconductor and MOFs in order to improve their photocatalytic performance and long-term stability.

As a classic MOFs, NH_2-MIL-125(Ti) is constructed from Ti_8O_8 clusters and 2-aminoterephthalic acid (ATA) linkers, which has attracted extensive interests due to its high surface area, excellent chemical stability and good photocatalytic activity under the irradiation of visible light [39,40]. And the metal-free semiconductor of g-C_3N_4 has been widely investigated as a photocatalyst due to its desired band-gap width (2.85 eV), appropriated band-edge positions, large surface area, fast charge transfer, excellent chemical stability, and low cost [41]. However, to the best of our knowledge, there were no reports on the combination of NH_2-MIL-125(Ti) with metal-free semiconductors to form a novel composite photocatalyst.

In this present work, in order to obtain a novel composite photocatalyst of metal-free semiconductor/MOFs, we combined the MOFs of NH_2-MIL-125(Ti) with g-C_3N_4 functionalized by benzoic acid (hereafter named as CFB) to synthesize a novel composite catalyst of CFB/NH_2-MIL-125(Ti) (hereafter named as CFBM) by a chemical method. Noteworthily, among the composite catalyst, the MOFs of NH_2-MIL-125(Ti) is covalently linked with the g-C_3N_4 nanosheets functionalized by benzoic acid because the carboxylate groups of the benzoic acid on the g-C_3N_4 nanosheets can be coordinated with the Ti ions of the NH_2-MIL-125(Ti). And the benzoic acid in the CFBM acts as electron mediator to form a novel Z-scheme photocatalyst with rapid separation rate of photogenerated electrons and holes, which is different from the cases that RGO or noble metals serves as electron mediator reported in the literatures, such as Cu_2O/Cu/AgBr/Ag, CdS/Au/$BiVO_4$ and g-C_3N_4/RGO/Bi_2MoO_6 [42–44]. Herein, we systematically studied the photocatalytic H_2 production from water splitting over the novel Z-scheme composite catalyst of CFB/NH_2-MIL-125(Ti), as well as the formation mechanism and the photocatalytic enhancement mechanism of the CFBM. The CFBM shows much better stability and higher photocatalytic activity for H_2 production than that of pure NH_2-MIL-125(Ti). The present work not only reports a novel Z-scheme catalyst with good stability and high photocatalytic activity for H_2 evolution from water splitting, but also proposes a new synthetic method to prepare the composite catalysts of metal-free semiconductor/MOFs, among which MOFs are linked with semiconductors via covalent bonds.

2. Experiment section

2.1. Syntheses

All of the chemicals were commercially obtained and used without further purification.

2.1.1. Synthesis of g-C_3N_4 nanosheets

g-C_3N_4 nanosheets was synthesized by thermal oxidation method according to the previous work [45]. Bulk g-C_3N_4 was obtained by heating thiourea (Aldrich, 99%) at 550 °C for 2 h.The g-C_3N_4 nanosheets were synthesized by thermal strip oxidation method, in which grinded bulk g-C_3N_4 powders were put into an open ceramic at 500 °C for 2 h with a heating rate of 2 °C/min. The final light yellow powder of g-C_3N_4 nanosheets was obtained.

2.1.2. Synthesis of benzoic acid functionalization of g-C_3N_4 nanosheets

Chemical grafting modification method was used to prepare benzoic acid functionalization of g-C_3N_4 nanosheets (CFB).

The phenyl carboxylic diazonium salt was pre-fabricated through the following steps [46]: 7 mmol of sodium hydroxide and 960 mg of 4-aminobenzoic acid were added to water and stirred to complete dissolution. Then, 7.6 mmol of sodiumnitrite was slowly added to the above solution under the temperature maintained at 0–5 °C. This solution was rapidly added to 6 mL HCl solution with concentration of 20% and stirred for 45 min.

The prepared g-C_3N_4 nanosheets was added to the deionized water and treated by ultrasound for 1 h. The as-synthesized diazonium salt was added to the g-C_3N_4 nanosheets suspension solution, and was stirred for 4 h at 0–5 °C in ice bath. Finally, the solution was filtered and washed several times with distilled water, ethanol, DMF, and acetone, respectively. The final powder was dried at 60 °C for 12 h under vacuum.

2.1.3. Synthesis of NH_2-MIL-125(Ti)

NH_2-MIL-125(Ti) was synthesized by a modified method reported in the literature [47]. 2-aminoterephthalic acid (ATA) (0.5 g, 3 mmol) was added into a dimethylformamide (DMF) (9 mL) and MeOH (1 mL) solution under magnetic stirring. And then tetra-*n*-butyl titanate Ti $(OC_4H_9)_4$ (0.26 mL, 0.75 mmol) was also added into the above mixed solution and stirred at room temperature for 30 min. Then the mixed solution was transferred into a 50 mL Teflon liner and maintained at 150 °C for 72 h. Finally, the purified product was washed several times by DMF and MeOH, and vacuum dryied overnight at 60 °C.

2.1.4. Synthesis of the CFBM composites

The synthetic process of CFB/MOFs composites is similar to that of pure NH_2-MIL-125(Ti). A certain amount of CFB powder was dispersed into DMF with the aid of ultrasonication. Then a mixture of DMF (5 mL), ATA (0.5 g), CFB/DMF mixture (4 mL), methanol (1 mL), and Ti $(OC_4H_9)_4$ (0.26 mL) was subjected to solvothermal conditions in a Teflon-lined stainless-steel autoclave for 72 h at 150 °C. After reaction, the resultant precipitate was separated by centrifugation, and washed repeatedly with DMF and methanol. Finally, the samples were dried at 60 °C under vacuum. Hereafter, the obtained samples of CFB/MOFs composed of 5, 10, 15, and 20% CFB (wt%) were denoted as 5CFBM, 10CFBM, 15CFBM, and 20CFBM, respectively.

2.1.5. Synthesis of 10wt%g-C_3N_4/MOFs heterostructured hybrids

The synthetic process of 10wt%g-C_3N_4/MOFs is same to that of 10CFBM except that CFB was replaced by g-C_3N_4.

2.2. Materials and measurements

The crystal phase was determined by X-ray diffraction (Bruker D8 CEVANCE) using graphite monochromatized Cu-*Ka* (λ = 1.5406 Å) radiation. The XRD data for indexing and cell-parameter calculations were collected in a scan mode with a scanning speed of 2°/min in the 2θ range between 5° and 70°. Optical properties were analyzed by using UV–vis diffuse reflectance spectra (DRS, Varian Cary 300) and photoluminescence spectra (F-7000, Hitachi, Japan) at room temperature. Raman spectra were recorded on a microscopic confocal Raman spectrometer (JY LabRam HR800) with a laser source of 785 nm for excitation. Electrochemical Impedance Spectroscopy (EIS) was carried out in Na_2SO_4/$K_3(Fe(CN)_6)$/$K_4(Fe(CN)_6)$ (Na_2SO_4 0.5 M, $K_3(Fe(CN)_6)$ 0.25 mM and $K_4(Fe (CN)_6)$ 0.25 mM) solution over the frequency ranging from 0.01 Hz to 100 kHz at 0.24 V, and the amplitude of the applied sine wave potential in each case was 5 mV. Fourier transformed infrared (FTIR) spectra of the samples were performed by a VERTEX-70 spectrometer, and KBr was used as a blank control. Brunauer–Emmett–Teller (BET) surface area of samples were measured by means of N_2 adsorption over a NOVA 2000e (Quantachrome) equipment. The element composition of catalysts was identified by X-ray photoelectron spectroscopy (XPS) (VG 250 Escalab spectrometer and Al-K = 1486.7 eV).

Electrochemical measurements were performed on a CHI 660D electrochemical workstation (Shanghai Chenhua, China) using a standard three-electrode cell with a working electrode, a standard calomel electrode as reference electrode, and a graphite electrode as counter electrode. Then the samples were dip-coated onto a 1 cm × 1 cm fluorine-tin oxide (FTO) glass electrode. 0.5 M Na2SO4 was used as the electrolyte.

2.3. Test of photocatalytic activity

As shown in Fig. S1 in ESI, all photocatalytic H_2 evolution experiments were performed via a Pyrex top-irradiation reaction vessel connected to a glass closed gas system (Prefect Light, Beijing, Labsolar-III (AG) in a Pyrex flask). A 300 W Xe lamp (Perfect light PLS-SXE300C; Wavelength range: 320 nm ≤ λ ≤ 780 nm, light intensity: 160 mW/cm^2) was used as the simulated sunlight source. The as-prepared catalyst (20 mg) was uniformly dispersed by using a magnetic stirrer in 80 mL of aqueous solution (containing H_2O/triethanolamine, v/v = 72:8). Then 3% Pt nanoparticles were deposited on NH_2-MIL-125(Ti) as cocatalysts, which were rooted in H_2PtCl_6 by a photodeposition method. The system was vacuum-treated several times to remove the dissolved air. The visible-light (> 420 nm) irradiation by a cutoff filter was used to photocatalytic splitting water, and then the amount of produced hydrogen was analyzed by an online gas chromatograph (GC7900). Meanwhile, the cooling water was used to maintain the temperature at 6 °C.

3. Results and discussion

3.1. Characterizations

Fig. 1a shows the XRD patterns of pure g-C_3N_4, CFB, NH_2-MIL-125(Ti), and the CFBM composites with different contents of CFB. The diffraction peaks of the pure g-C_3N_4 and NH_2-MIL-125(Ti) are consistent with those reported in the literatures [41,48]. And the peaks of CFB are nearly same to those of pure g-C_3N_4, indicating the modification of benzoic acid does not affect the crystal structure of g-C_3N_4. When the doping amount of CFB is smaller than 10%, the characteristic peaks of CFB cannot be clearly observed in the XRD pattern of the CFBM. With the increase of the amount of CFB, the characteristic peaks of CFB at 27.6° can be clearly observed in the XRD pattern of the CFBM. This could be due to the intensities of the peaks at 27.6° and 13.5° of CFB much weaker than that of the pure NH_2-MIL-125(Ti). In addition, the new characteristic peaks of the CFBM composites at 18.9°, 20.5° and 24.8° could be resulted from the fact that MOFs are linked with the doped CFB via covalent bonds to form a composite with similar structure of NH_2-MIL-125(Ti) [49].

As shown in Fig. 1b, it describes the FTIR spectra of the as-prepared samples. The g-C_3N_4 nanosheets have five characteristic peaks at 810, 1245, 1324, 1458, and 1642 cm^{-1}, which are assigned to the stretching vibrations of tri-s-triazine ring units. The FTIR spectrum of CFB has a strong characteristic peak of the C=O stretch at 1628 cm^{-1}, demonstrating that the surface of the g-C_3N_4 nanosheets is rich in carboxyl groups. Besides, the characterized fingerprint at 1571 cm^{-1} is ascribed to the phenyl C=C ring stretch of the benzoic acid. The FTIR spectrum of NH_2-MIL-125(Ti) shows characteristic peaks at 1434 cm^{-1} and 1656 cm^{-1} that are attributed to symmetrical stretching vibration of carboxylates groups, and O-Ti-O vibrations exhibit in 400–800 cm^{-1} [15]. The FTIR spectrum of 10CFBM is similar to that of NH_2-MIL-125(Ti) but the wavenumber of C=O red-shifts from 1656 cm^{-1} at NH_2-MIL-125(Ti) to 1628 cm^{-1} at 10CFBM, further confirming that the CFB participates in the synthesis of CFBM by the bidentate coordination of the carboxylate group with the titanium clusters in MOFs.

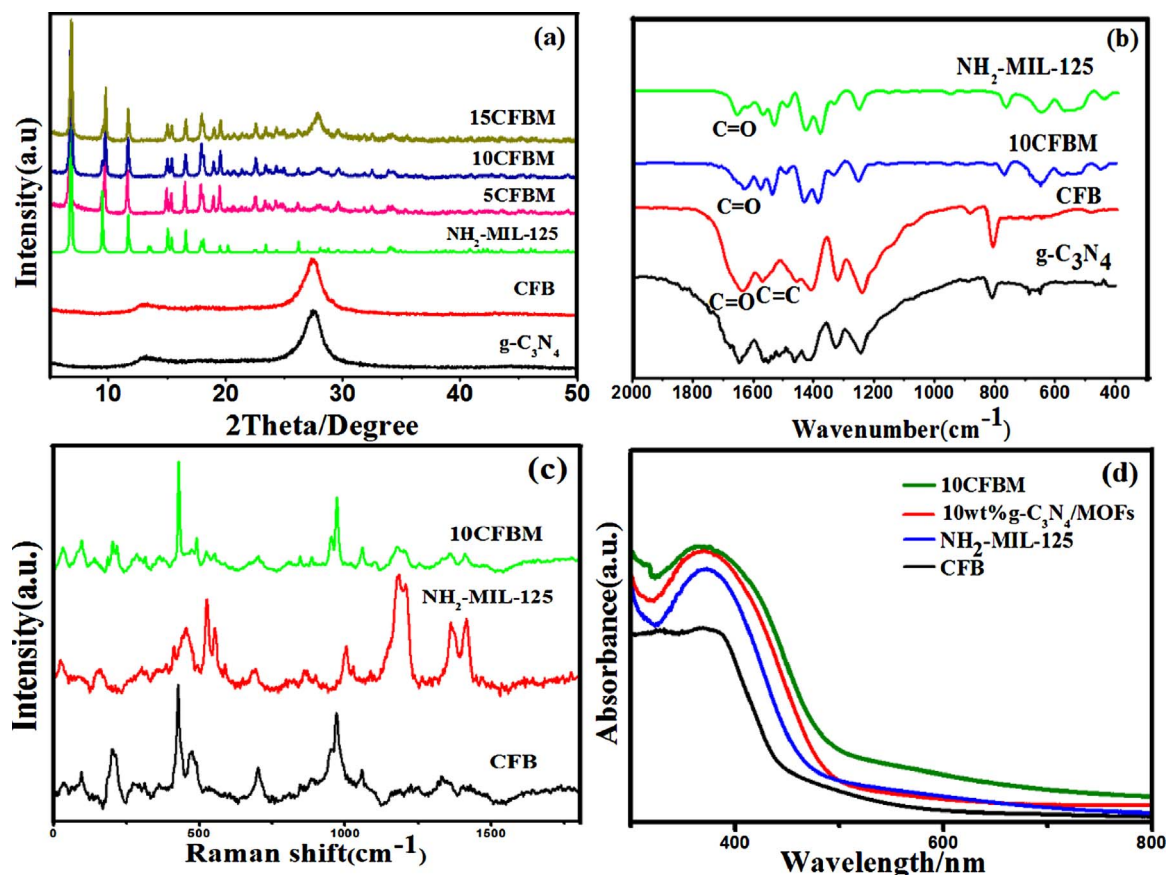In order to confirm the existence of CFB sheets in the CFBM

Fig. 1. XRD patterns (a); FTIR spectra (b); Raman spectra (c); and UV–vis absorption spectra (d) of the as-prepared catalysts.
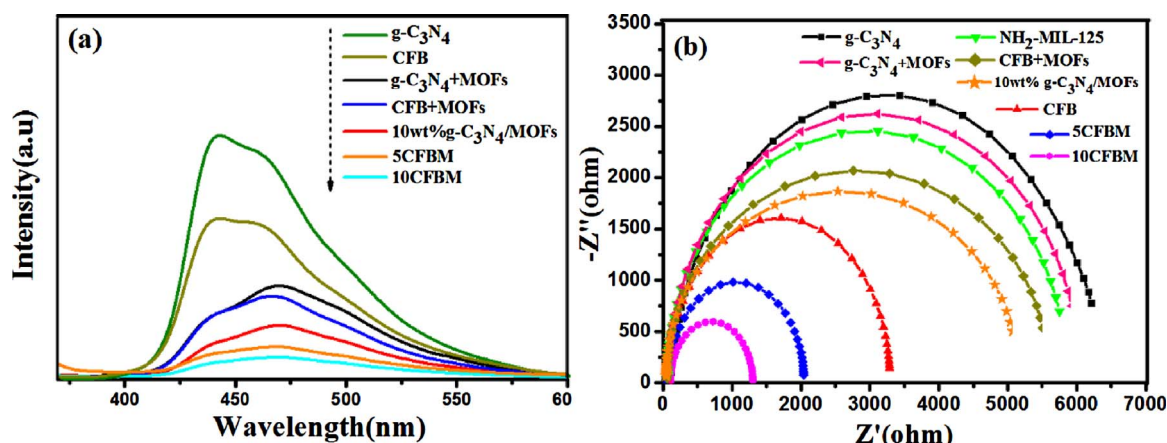
Fig. 2. PL spectra of the as-prepared catalysts at an excitation wavelength of 325 nm (a); Electrochemical impedance spectra of the as-prepared catalysts (b).

composite, Raman spectra were investigated. As shown in Fig. 1c, the main vibration bands of pure NH_2-MIL-125(Ti) can be clearly observed in the Raman spectra at 524, 1177, 1360, and 1413 cm^{-1}. When NH_2-MIL-125(Ti) was linked with CFB via covalent bonds, the characteristic peaks of CFB (205, 427, 701, and 970 cm^{-1}) and the MOFs (524, 1177, 1360, and 1413 cm^{-1}) were also observed in the 10CFBM composites but the intensity of these characteristic peaks became weaker than those in CFB and MOFs. The results demonstrate that the CFB exists in the 10CFBM composites and there could be covalent bonds to link the CFB and MOFs among the 10CFBM composites. The optical properties of the samples were studied by the UV–vis absorption spectra. As shown in Fig. 1d and Fig. S2, the absorption edge at about 500 and 450 nm belongs to the NH_2-MIL-125(Ti) and CFB, respectively. Compared with the pure NH_2-MIL-125(Ti) and CFB, the 10CFBM has much stronger absorption intensity in the visible light region and the absorption edge obviously red-shifts. Fig. 2a shows PL spectra of pure g-C_3N_4 nanosheets, CFB, 5CFBM and 10CFBM samples measured at an excitation wavelength of 325 nm. The higher PL peak means higher recombination rate of photogenerated electrons and holes, leading to lower photocatalytic activity. Among the as-prepared catalysts (the g-C_3N_4, CFB, 5CFBM, and 10CFBM), the PL intensity of the 10CFBM is the smallest one, showing 10CFBM has the lowest recombination rate of photogenerated electrons and holes, which results in the best photocatalytic performance. To assess the efficiency of charge transfer of the samples, the electrochemical impedance spectroscopy (EIS) measurements were investigated. As shown in Fig. 2b, 10CFBM shows the smallest resistance among the as-prepared catalysts, indicating that the best efficient charge separation occurred in the 10CFBM, which confirms that the introduction of CFB is very helpful for the improvement of photocatalytic performance of the NH_2-MIL-125(Ti) [6].

The morphologies of NH_2-MIL-125(Ti) and CFBM can be observed via SEM and TEM images presented in Fig. 3. The NH_2-MIL-125(Ti) exhibits granular structure (Fig. 3a). When combined with CFB, the morphologies of NH_2-MIL-125(Ti) have a little change (Fig. 3b), indicating that the NH_2-MIL-125(Ti) are linked with a certain amount of g-C_3N_4 via covalent bonds. When the amount of CFB is larger than 10 wt% (Fig. 3c), many nanosheets of CFB were covered on the surface of NH_2-MIL-125(Ti), showing the amount of CFB nanosheets in the CFBM composites has a significant effect on the formation of CFBM composites. The TEM of 10CFBM (Fig. 3d) also demonstrates that there are good contacts of NH_2-MIL-125(Ti) with g-C_3N_4.

As shown in Table S1 and Fig. S3, BET of the CFB and NH_2-MIL-125(Ti) are found to be 26.5 $m^2 g^{-1}$ and 1260.3 $m^2 g^{-1}$, respectively, while that of 10CFBM is 269.2 $m^2 g^{-1}$, indicating the MOFs of NH_2-MIL-125(Ti) could be linked with CFB via covalent bonds and then leads to the decrease of BET of the MOFs.

X-ray photoelectron spectroscopy (XPS) was used to determine the interactions between MOFs and CFB in the 10CFBM (Fig. 4a–d). Fig. 4a shows the wide-scan XPS spectra of the CFB, NH_2-MIL-125(Ti) and 10CFBM, indicating the existence of C, N, O, and Ti elements in the 10CFBM. As for CFB, three peaks at 289.0, 400.2 and 532.8 eV are assigned to C 1s, N 1s, and O 1s, respectively, indicating the existence of C, N, and O elements, demonstrating there are some carboxylic groups on the surface of g-C_3N_4 among the CFB [25].

The C 1 s spectra of CFB, NH_2-MIL-125(Ti) and 10CFBM samples displays in Fig. 4b. As for CFB, three peaks centering at 284.5, 285.3, and 288.5 eV can be assigned to C=C, C−N and C=O bonds, respectively, indicating that the carboxylic groups exist on the surface of g-C_3N_4. The C 1 s spectra of NH_2-MIL-125(Ti) and 10CFBM have four similar peaks at 288.5, 286.3, 285.3 and 284.5 eV but the peak of C−N in the 10CFBM has much higher intensities than that in NH_2-MIL-125(Ti), indicating that CFB was involved in the growth of the MOF crystals. The results are also in good agreement with the aforementioned Raman spectra analysis. Fig. 4c shows the N 1 s spectrum of 10CFBM. The spectrum can be deconvoluted into three peaks, which can be ascribed to C−N=C at 398.6 eV, N-(C)₃ at 399.6 eV, and graphitic-N species (-NH-⁺) at 402.1 eV, respectively [25]. As shown in Fig. 4d, peaks at 458.8 and 464.5 eV are assigned to the Ti $2p_{3/2}$, and Ti $2p_{1/2}$ of 10CFBM, respectively, showing valence state of titanium remains unchanged after the MOF of NH_2-MIL-125(Ti) was covalently bonded with CFB before the photocatalytic reaction, which is consistent with the case in the titanium-oxo cluster [50]. In addition, after 2 h photocatalytic reaction, a new peak appeared at 457.8 eV for the Ti 2p3/2 that is assigned to Ti^{3+}, demonstrating that the valence state transformation of Ti^{4+} to Ti^{3+} occurred in the process of photocatalytic reaction.

3.2. Photocatalytic H_2 production

The photocatalytic H_2 production activities of the as-prepared samples were studied in aqueous solution under the irradiation of visible light ($\lambda \geq 420$ nm) using triethanolamine as sacrificial agents, and Pt nanoparticles was in situ photo-loaded as cocatalyst. Control experiments show no H_2 production in the absence of photocatalysts or light illumination. As shown in Fig. 5a and c, the NH_2-MIL-125(Ti) and g-C_3N_4 show a low photocatalytic H_2-production rate of 0.187 and 0.688 mmol·h^{-1}·g^{-1}, respectively. As for CFB, it has a higher H_2 production rate (0.816 mmol·h^{-1}·g^{-1}) than the g-C_3N_4, indicating that the carboxylic groups on the surface of CFB can improve the photocatalytic activity of g-C_3N_4. In order to improve the photocatalytic activities of pure MOFs, it was combined with CFB. As shown in Fig. 5b, after the coupling of CFB, the H_2 production rate of the NH_2-MIL-125(Ti) was markedly improved. With the increase of the amount of CFB, the H_2 production rate of CFBM increases. However, when the amount of CFB
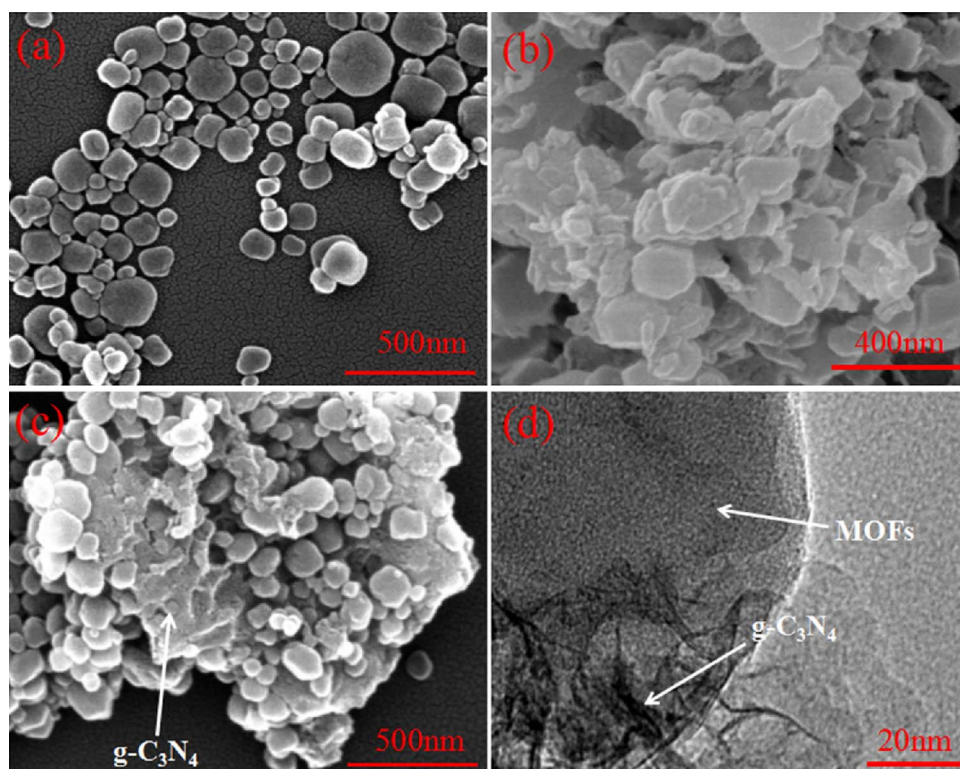
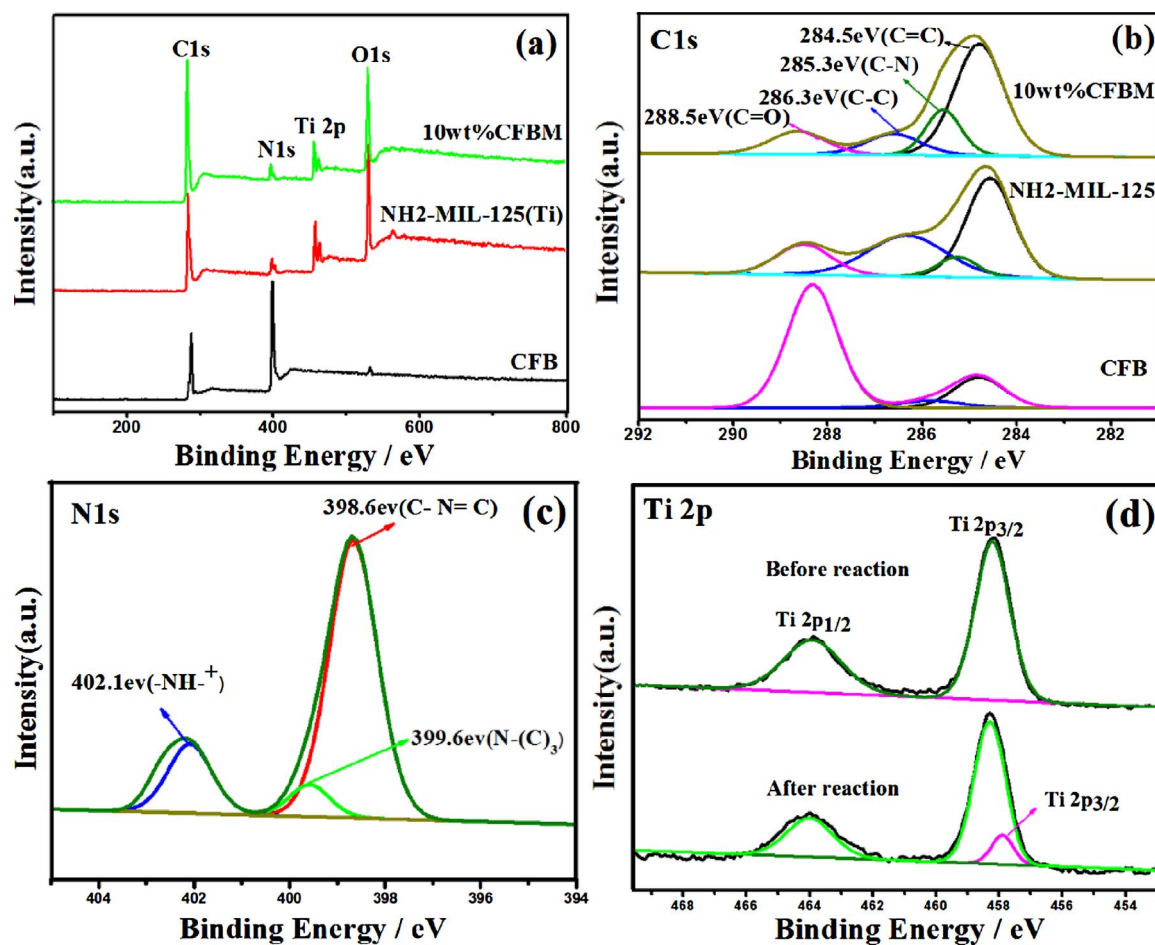**Fig. 3.** SEM images of NH$_2$-MIL-125(Ti) (a), 10CFBM (b) and 15CFBM (c); and TEM images of 10CFBM (d).

Fig. 4. XPS survey spectra (a) and high-resolution XPS of spectra of C 1 s (b) and N 1 s (c) of the CFB, MOF and 10CFBM; and Ti 2p (d) of 10CFBM before and after 2 h photocatalytic reaction.
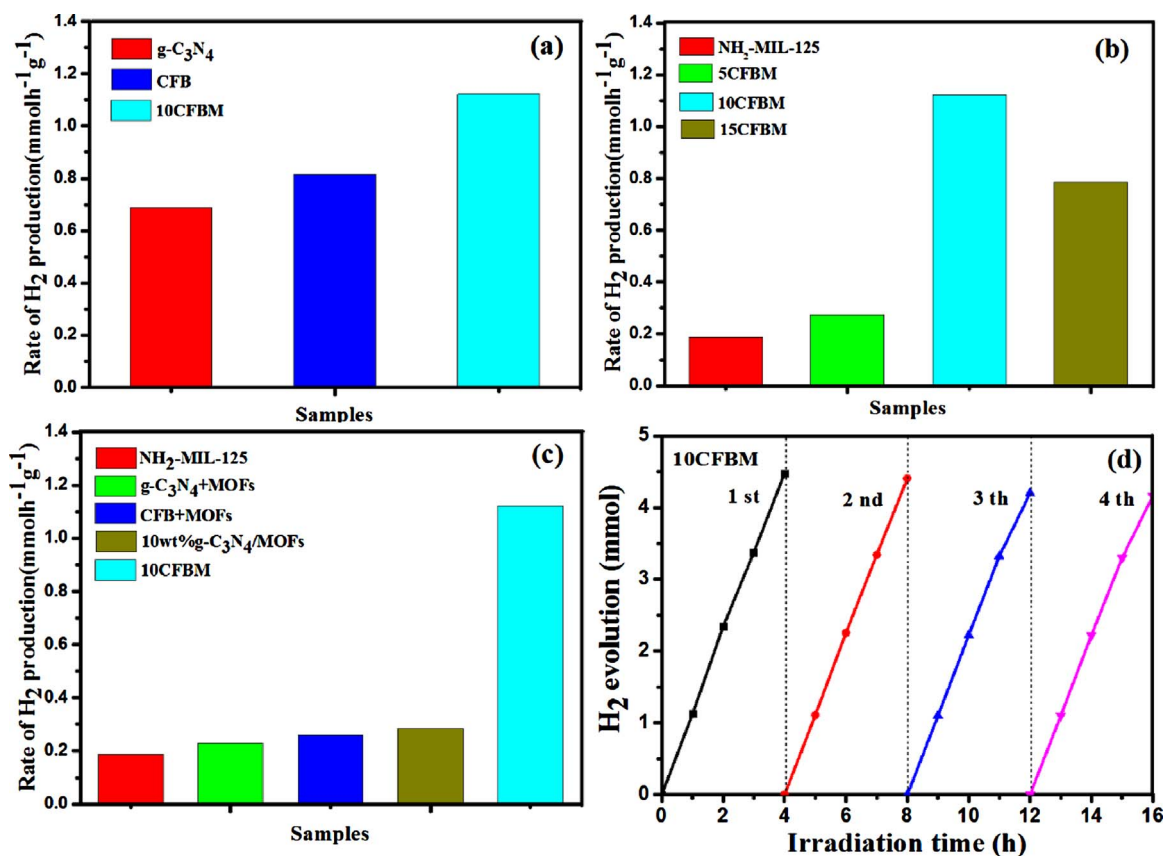
Fig. 5. The rate of hydrogen evolution over the different samples under visible light irradiation (a–c). The cycling runs of 10CFBM catalyst under visible light irradiation for 16 h (d).

is larger than 10 wt%, the H_2 production rate decreases, which could be due to more CFB coating on the NH_2-MIL-125(Ti) surface resulting in worse light absorption and photocatalytic activity. Therefore, an appropriate amount of CFB linked with MOFs via covalent bonds is important to achieve the optimal H_2 production rate of the CFBM composite catalysts. The optimal amount of CFB is 10 wt% and the H_2 production rate of the 10CFBM is 1.123 mmol·h^{-1}·g^{-1}, which is about 6 times of the NH_2-MIL-125(Ti). The results confirm that the combination of MOFs and CFB via covalent bonds can efficiently depress the recombination of photogenerated electron-hole in the CFBM composite catalysts, thereby leading to the enhancement of H_2 production rate. The results are also in good agreement with the above-mentioned PL and EIS results. All in all, the above results clearly reveal the CFB is vital to enhancing the photocatalytic performance of H_2 production of MOFs via forming a novel kind of metal-free semiconductor/MOFs heterostructured catalyst by covalent bonds.

In order to well study whether the CFBM is a Z-scheme heterostructured catalyst, some control experiments has been done. As presented in Fig. 5c, the simple physical mixture of NH_2-MIL-125(Ti) with 10 wt% g-C_3N_4 and the 10wt%g-C_3N_4/MOFs heterostructured catalyst show a H2 evolution rate of 0.23 mmol·h^{-1}·g^{-1} and 0.28 mmol·h^{-1}·g^{-1}, respectively, while the simple physical mixture of NH_2-MIL-125(Ti) and 10 wt% CFB shows a H2 evolution rate of 0.26 mmol·h^{-1}·g^{-1}. The H2 evolution rates of the three kinds of samples are all much smaller than that of the 10CFBM (1.123 mmol·h^{-1}·g^{-1}), indicating the CFBM could be a Z-scheme heterostructured catalyst but not a simple heterostructured catalyst consisted of g-C_3N_4 and MOF. Among the CFBM, the carboxylic oxygen atoms of CFB are bonded with the Ti of the NH_2-MIL-125(Ti), leading to the benzoic acid as a bridge between MOFs and g-C_3N_4 to form a good electronic transmission channel that can efficiently enhance the photocatalytic activity for photocatalytic H_2 production from water splitting. To the best of our knowledge, different from the conventional Z-

scheme heterostructured catalysts that consist of noble metals or graphene as electronic transmission channel, the CFB/MOFs is the first case that rigid organic ligand plays the role of electronic transmission channel to establish a novel Z-scheme heterostructured catalyst.

The lifetime and stability of the 10CFBM was also investigated. As depicted in Fig. 5d, after four recycles, the photocatalytic H_2 evolution rate of the 10CFBM nearly became unchanged, implying that the sample has good stability and long lifetime in the photocatalytic hydrogen production process. In contrast, after four recycles, the photocatalytic H_2 evolution rate of the 10wt%g-C_3N_4/MOFs heterostructured catalyst markedly decreased from 0.28 to 0.192 mmol·h^{-1}·g^{-1} (Fig. S4). The results prove that the novel Z-scheme heterostructured catalyst of 10CFBM formed by covalent bond exhibits much better lifetime and stability than that of the conventional heterostructured catalyst of 10wt%g-C_3N_4/MOFs formed by weak van der Waals force.

3.3. Formation mechanism of the CFBM

On the basis of the structural analysis, a growth mechanism of CFBM was proposed. As shown in Scheme 1, the synthesis strategy employed in this study involves two steps: g-C_3N_4 functionalized by benzoic acid (CFB) and in situ growth of CFBM. Firstly, the g-C_3N_4 nanosheets were functionalized by benzoic acid to form the CFB. And then the Ti^{4+} is simultaneously bridged by carboxylate groups of CFB and the deprotonated 2-aminoterephthalic acid via in situ hydrothermal reaction, resulting in the three-dimensional channel structure of CFBM, among which the MOFs of NH_2-MIL-125(Ti) are linked with the benzoic acid functionalization of g-C_3N_4 via covalent bonds [46]. The as-prepared CFBM is similar to the report in the literature that MOFs was covalently linked with graphene to form a novel composite catalyst [49].
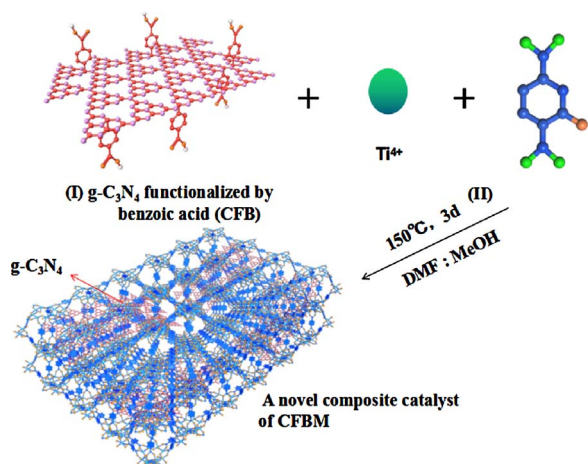
Scheme 1. Schematic representation of the synthesis of covalently linked CFBM composites. (I) g-C$_3$N$_4$ functionalized by benzoic acid (CFB) and (II) in situ growth of CFBM crystals.

3.4. Possible photocatalytic mechanism of the Z-scheme 10CFBM

In order to research the enhancement mechanism of the photocatalytic activity of the composite CFBM, UV–vis diffuse reflection spectra (DRS) and Mott-Schottky plots of the NH$_2$-MIL-125(Ti) and g-C$_3$N$_4$ were investigated. As shown in Fig. S5a, the DRS spectra of the as-prepared NH$_2$-MIL-125(Ti) and g-C$_3$N$_4$ show that the calculated band gaps of NH$_2$-MIL-125(Ti) and g-C$_3$N$_4$ are 2.60, and 2.85 eV, respectively. Fig. S5b shows the Mott-Sckottky (MS) plots with NH$_2$-MIL-125(Ti) and g-C$_3$N$_4$ being working electrode (0.5 M K$_2$SO$_4$ as electrolyte). The flat band potential (V$_{fb}$) as calculated from the x intercepts of the linear region are found to be −1.36 and −0.74 eV vs SCE (equivalent to 1.12, and 0.50 eV vs. NHE, respectively) for NH$_2$-MIL-125(Ti) and g-C$_3$N$_4$, respectively. It is known that the flat band potential of n-type semiconductor equals to the Fermi Level (E$_F$). Therefore, the E$_F$ values of NH$_2$-MIL-125(Ti) and g-C$_3$N$_4$ are 1.12, and 0.50 eV, respectively. Accordingly, the CB of NH$_2$-MIL-125(Ti) and g-C$_3$N$_4$ can be calculated as −1.32 and −0.70 eV, respectively [51,52]. The band positions can be calculated by the following empirical formulas: E$_{CB}$ = E$_{VB}$ − E$_g$, and the valence band (VB) of NH$_2$-MIL-125(Ti) and g-C$_3$N$_4$ are 1.28 and 2.15 eV, respectively.

On the basis of the above experimental results, we proposed the mechanism of the photocatalytic hydrogen production over the novel Z-scheme catalyst of 10CFBM. As shown in Scheme 2, under irradiation of visible light, the g-C$_3$N$_4$ and the MOFs of NH$_2$-MIL-125(Ti) can directly absorb light of 420–480 nm to generate electrons (e$^-$) and holes (h$^+$)
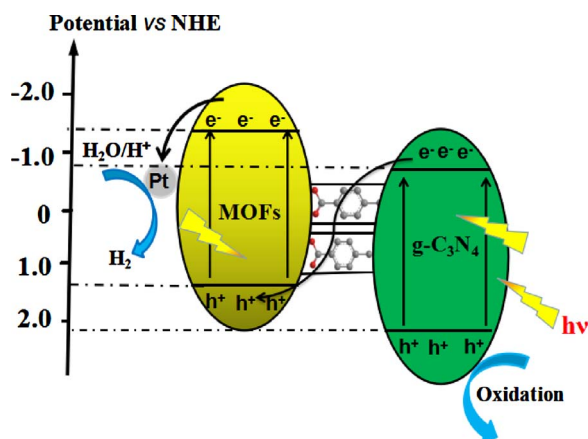
and the electrons are excited from the VB to CB. Firstly, the photogenerated electrons on the CB of the MOFs transfer to Pt nanoparticles deposited on the surface of the MOFs and then are reacted with H$_2$O to produce H$_2$, whereas the photogenerated electrons on the CB of g-C$_3$N$_4$ recombine with the photogenerated holes on the VB of MOFs via benzoic acid as an electron mediator, leading to the excellent separation of photogenerated electrons on the MOFs and holes on the g-C$_3$N$_4$. Meanwhile, the holes on the VB of g-C$_3$N$_4$ are reacted with the sacrificial agent of triethanolamine to finish the oxidation process, which improves the separation of photogenerated electrons and holes. Secondly, the organic linker of 2-aminoterephthalic acid can absorb visible light to generate an excited state of 2-aminoterephthalic acid and electrons due to its good photosensitivity, and then the electrons are transferred to the titanium-oxo cluster in the manner of LCCT mechanism, leading to the formation of Ti^{3+} species. Furthermore, H$_2$ would be produced when Ti^{3+} is reacted with H$_2$O during the process of the transformation between Ti^{3+} to Ti^{4+} that was demonstrated by the XPS results (Fig. 4d), which is consistent with the case reported in the literature [48]. The proposed mechanism well explains why the novel Z-scheme system has excellent photocatalytic H$_2$ evolution from water.

4. Conclusions

We proposed a new synthetic method to prepare a novel Z-scheme heterostructured catalyst of metal-free semiconductor/MOFs, among which the MOFs of NH$_2$-MIL-125(Ti) are linked with the benzoic acid functionalization of g-C$_3$N$_4$ via covalent bonds. The CFB linked with MOFs via covalent bonds not only increases the stability of the heterostructured catalyst of 10CFBM but also improve the electron transfer rate between g-C$_3$N$_4$ and NH$_2$-MIL-125(Ti). Meanwhile, the matched energy level of g-C$_3$N$_4$ and the MOFs of NH$_2$-MIL-125(Ti) makes the excellent separation of photogenerated electrons and holes, leading to good photocatalytic performance of H$_2$ evolution from water splitting. Therefore, our present work not only reported a new kind of metal-free semiconductor/MOFs with excellent photocatalytic performance for H$_2$ evolution from water splitting but also proposed a new strategy to build up a novel Z-scheme heterostructured catalyst of semiconductor/MOFs. A mechanism was put forward to explain the role of benzoic acid in the Z-scheme heterostructured catalyst and the excellent photocatalytic performance of the CFBM.

Scheme 2. Photocatalytic mechanism of the charge transfer for hydrogen evolution over the 10CFBM under visible light irradiation.

Appendix A. Supplementary data

Supplementary data associated with this article can be found, in the online version, at http://dx.doi.org/10.1016/j.apcatb.2017.08.086.

References

[1] W. Mtangi, F. Tassinari, K. Vankayala, A. Vargas Jentzsch, B. Adelizzi, A.R. Palmans, C. Fontanesi, E.W. Meijer, R. Naaman, J. Am. Chem. Soc 139 (2017) 2794–2798.

[2] X. Hao, Z. Jin, H. Yang, G. Lu, Y. Bi, Appl. Catal. B: Environ. 210 (2017) 45–56.

[3] J.P. Zou, L.C. Wang, J.M. Luo, Y.C. Nie, Q.J. Xing, X.B. Luo, H.M. Du, S.L. Luo, L. Steven Suib, Appl. Catal. B Environ. 193 (2016) 103–109.

[4] S. Zhang, L. Wang, C. Liu, J. Luo, J. Crittenden, X. Liu, T. Cai, J. Yuan, Y. Pei, Y. Liu, Water Res. 121 (2017) 11–19.

[5] L.J. Shen, Y.H. Liu, R.W. Liang, F.F. Jing, L. Wu, Appl. Catal. B: Environ. 56 (2014) 0926–3373.

[6] R. Lin, L. Shen, Z. Ren, W. Wu, Y. Tan, H. Fu, J. Zhang, L. Wu, Chem. Commun. 50 (2014) 8533–8535.

[7] J.P. Zou, S.L. Lei, J. Yu, S.L. Luo, X.B. Luo, X.H. Tang, W.L. Dai, J. Sun, G.C. Guo, C.T. Au, Appl. Catal. B: Environ. 150–151 (2014) 466–471.

[8] K. Li, M. Han, R. Chen, S.L. Li, S.L. Xie, C. Mao, X. Bu, X.L. Cao, L.Z. Dong, P. Feng, Y.Q. Lan, Adv. Mater. 28 (2016) 8906–8911.

[9] T. Song, L. Zhang, P.Y. Zhang, J. Zeng, T.T. Wang, Atif Ali, H.P. Zeng, J. Mater. Chem. A 5 (2017) 6013–6018.

[10] W. Wang, X.M. Xu, W. Zhou, Z.P. Shao, Adv. Sci. 4 (2017) 1600371.

[11] C. Liu, L. Wang, Y. Tang, S. Luo, Y. Liu, S. Zhang, Y. Zeng, Y. Xu, Appl. Catal. B: Environ. 164 (2015) 1–9.

[12] Y. Li, L. Wang, T. Cai, S. Zhang, Y. Liu, Y. Song, X. Dong, L. Hu, J Chem Eng 321 (2017) 366–374.

[13] T. Cai, Y. Liu, L. Wang, S. Zhang, Y. Zeng, J. Yuan, J. Ma, W. Dong, C. Liu, S. Luo, Appl. Catal. B: Environ. 208 (2017) 1–13.

[14] L.G. Gordeeva, M.V. Solovyeva, Y.I. Aristov, Energy 100 (2016) 18–24.

[15] Z.H. Rada, H.R. Abid, J. Shang, Y. He, P. Webley, S. Liu, H. Sun, S. Wang, Fuel 160 (2015) 318–327.

[16] M.A. Nasalevich, R. Becker, E.V. Ramos-Fernandez, S. Castellanos, S.L. Veber, M.V. Fedin, F. Kapteijn, J.N.H. Reek, J.I. van der Vlugt, J. Gascon, Energy Environ. Sci. 8 (2015) 364–375.

[17] Y. Zhang, B. Fu, K. Liu, Y. Zhang, X. Li, S. Wen, Y. Chen, S. Ruan, Sens. Actua B: Chem. 201 (2014) 281–285.

[18] X. Kang, Q. Zhu, X. Sun, J. Hu, J. Zhang, Z. Liu, B. Han, Chem. Sci. 7 (2016) 266–273.

[19] S. Zhong, Q. Wang, D. Cao, Sci. Rep. 6 (2016) 21295.

[20] X. Luo, Y. Cao, T. Wang, G. Li, J. Li, Y. Yang, Z. Xu, J. Zhang, Q. Huo, Y. Liu, M. Eddaoudi, J. Am. Chem. Soc. 138 (2016) 786–789.

[21] L. Shi, T. Wang, H. Zhang, K. Chang, X. Meng, H. Liu, J. Ye, Adv. Sci. 2 (2015) 1500006.

[22] J.-L. Wang, C. Wang, W. Lin, ACS Catal. 2 (2012) 2630–2640.

[23] J. Zhang, J.T. Bu, S. Chen, T. Wu, S. Zheng, Y. Chen, R.A. Nieto, P. Feng, X. Bu, Angew. Chem. Int. Ed. 49 (2010) 8876–8879.

[24] R. Wang, L. Gu, J. Zhou, X. Liu, F. Teng, C. Li, Y. Shen, Y. Yuan, Adv. Mater. 2 (2015) 1500037.

[25] H. Wang, X. Yuan, Y. Wu, G. Zeng, X. Chen, L. Leng, H. Li, Appl. Catal. B: Environ. 174–175 (2015) 445–454.

[26] S. Wang, X. Wang, Appl. Catal. B: Environ. 162 (2015) 494–500.

[27] M. Wang, D. Wang, Z. Li, Appl. Catal. B: Environ. 183 (2016) 47–52.

[28] Q. Li, B. Guo, J. Yu, J. Ran, B. Zhang, H. Yan, J.R. Gong, J. Am. Chem. Soc. 133 (2011) 10878–10884.

[29] C.F. Zhang, L.G. Qiu, F. Ke, Y.J. Zhu, Y.P. Yuan, G.S. Xu, X. Jiang, J. Mater Chem A 1 (2013) 14329.

[30] S.T. Gao, W.H. Liu, N.Z. Shang, C. Feng, Q.H. Wu, Z. Wang, C. Wang, RSC Adv. 4 (2014) 61736–61742.

[31] X. Gu, Z.H. Lu, H.L. Jiang, T. Akita, Q. Xu, J. Am. Chem. Soc. 133 (2011) 11822–11825.

[32] C. Wang, K.E. de Krafft, W. Lin, J. Am. Chem. Soc. 134 (2012) 7211–7214.

[33] W.W.L.J. Shen, R.W. Liang, R. Lin, L. Wu, Nanoscale 5 (5) (2013) 9374–9382.

[34] L. Huang, B. Liu, RSC Adv. 6 (2016) 17873–17879.

[35] L. Wang, X. Liu, J. Luo, X. Duan, J. Crittenden, C. Liu, S. Zhang, Y. Pei, Y. Zeng, X. Duan, Angew. Chem. Int. Ed. 56 (2017) 7610–7614.

[36] L. Wang, X. Duan, G. Wang, C. Liu, S. Luo, S. Zhang, Y. Zeng, Y. Xu, Y. Liu, X. Duan, Appl. Catal. B: Environ. 186 (2016) 88–96.

[37] W.H. Dong, D.D. Wu, J.M. Luo, Q.J. Xing, H. Liu, J.P. Zou, X.B. Luo, X.B. Min, H.L. Liu, S.L. Luo, C.T. Au, J. Catal. 349 (2017) 218–225.

[38] J. Xu, S. He, H. Zhang, J. Huang, H. Lin, X. Wang, J. Long, J. Mater Chem A. 3 (2015) 24261–24271.

[39] Z. Su, J.H. Chen, X. Sun, Y. Huang, X. Dong, RSC Adv. 5 (2015) 99008–99017.

[40] M. Martis, K. Mori, K. Fujiwara, W.S. Ahn, H. Yamashita, J. Phys Chem C. 117 (2013) 22805–22810.

[41] X. Zhang, X. Xie, H. Wang, J. Zhang, B. Pan, Y. Xie, J. Am. Chem. Soc. 135 (2013) 18–21.

[42] J. He, D.W. Shao, L.C. Zheng, L.J. Zheng, D.Q. Feng, J.P. Xu, X.H. Zhang, W.C. Wang, W.H. Wang, F. Lu, H. Dong, Y.H. Cheng, H. Liu, R.K. Zheng, Appl. Catal. B: Environ. 203 (2017) 917–926.

[43] D. Ma, J. Wu, M. Gao, Y. Xin, Y. Sun, T. Ma, J. Chem. Eng. 313 (2017) 1567–1576.

[44] S.Y. Bao, Q.F. Wu, S.Z. Chang, B.Z. Tian, J.L. Zhang, Catal. Sci. Technol. 7 (2017) 124–132.

[45] W. Wang, J.C. Yu, Z. Shen, D.K. Chan, T. Gu, Chem. Commun. 50 (2014) 10148–10150.

[46] Maryam Jahan, Q.L. Bao, J.X. Yang, Kian JPing Loh, J. Am. Chem. Soc 132 (2010) 14487–14495.

[47] Y. Fu, D. Sun, Y. Chen, R. Huang, Z. Ding, X. Fu, Z. Li, Angew. Chem. Int. Ed. 51 (2012) 3364–3367.

[48] Y. Horiuchi, T. Toyao, M. Saito, K. Mochizuki, M. Iwata, H. Higashimura, M. Anpo, M. Matsuoka, J. Phys. Chem. C. 116 (2012) 20848–20853.

[49] R. Kumar, D. Raut, U. Ramamurty, C.N. Rao, Angew. Chem. Int. Ed. 55 (2016) 7857–7861.

[50] H. Wang, X. Yuan, Y. Wu, G. Zeng, X. Chen, L. Leng, Z. Wu, L. Jiang, H. Li, J. Hazard. Mater. 286 (2015) 187–194.

[51] J.P. Zou, S.L. Luo, L.Z. Zhang, J. Ma, S.L. Lei, L.S. Zhang, X.B. Luo, Y. Luo, G.S. Zeng, C.T. Au, Appl. Catal. B: Environ. 140–141 (2013) 608–618.

[52] J. Ding, Z. Dai, F. Qin, H. Zhao, S. Zhao, R. Chen, Appl. Catal. B: Environ. 205 (2017) 281–291.